Adamantanes enhance the photovoltaic performance and operational stability of perovskite solar cells by effective mitigation of interfacial defect states

Mohammad Mahdi Tavakoli[1,2], Dongqin Bi[1], Linfeng Pan[1], Anders Hagfeldt[1], Shaik Mohammed Zakeeruddin[1], Michael Grätzel[1]*

[1]*Institut des Sciences et Ingénierie Chimiques, Ecole Polytechnique Fédérale de Lausanne (EPFL), EPFL–BCH, CH–1015 Lausanne, Switzerland*

[2]*Present address: Department of Electrical Engineering and Computer Science, Massachusetts Institute of Technology, Cambridge, MA, USA*

* Corresponding author: michael.graetzel@epfl.ch

Passivation of electronic defects is an effective strategy to boost the performance and operational stability of perovskite solar cells (PSCs). Identifying molecular materials that achieve this purpose is a key target of current research efforts. Here we introduce adamantane (AD) and 1-adamantylamine (ADA) as molecular modulators to abate electronic defects present within the bulk and at the perovskite-hole conductor interface. To this effect, we have added the modulator either into the anti-solvent to precipitate it together with the perovskite (AS method) or we spin-coated them onto its surface (SC method). Time-resolved photoluminescence (TRPL) measurements show substantially longer lifetimes for perovskite films treated with AD (34.6 ns) and ADA (68.4 ns) compared to the reference sample (14.3 ns). In line with this observation we find that the presence of AD and ADA molecules at the interface between the perovskite film and the hole conductor increases all photovoltaic metrics, in particular the open circuit photovoltage (V_{oc}) as well as the operational stability of the PSC.

Introduction

Recent rapid progress in the field of perovskite solar cells (PSCs) has stimulated intensive world-wide research resulting in the current certified solar to electric power conversion efficiency (PCE) of 22.7%.[1-3] Presently, innovative device architectures, interface modulation, as well as compositional and crystal growth engineering are being employed to improve the device performance further and establish long term operational stability.[4-8] Mitigation of electronic defects plays a key role to reduce radiationless carrier recombination resulting in higher open circuit photovoltages (V_{oc}).[7,9] To this effect, the modulating agents are either added to the anti-solvent or the perovskite precursor solution.[10-13] A wide variety of additives has been examined, including polymers[14-16], fullerenes[17,18], metal halides[19-21], inorganic acids[22,23], co-solvents[24,25], organic halide salt[26-29], and nanoparticles.[30] Some of them can manipulate the film morphology and form uniform and smooth surfaces, while others enhance the optical and electrical properties of the perovskite layer. Chang *et al.*[31] added poly(ethylene glycol) (PEG) together with [6,6]-phenyl-C61-butyric acid methyl ester ($PC_{61}BM$) to the perovskite starting solution and showed their role in improving film coverage and charge transfer dynamics, enhancing the open circuit voltage (V_{oc}) as well as short current density (J_{sc}). Bi *et al.*[32] employed poly(methyl methacrylate) (PMMA) as a template by adding it into the anti-solvent to control the nucleation and growth of perovskite film. They found that the prepared film by this technique shows high quality with longer lifetime, resulting in a certified PCE of 21.0%. Zhang *et al.*[33] employed the same method and treated the surface of perovskite film by α-bis-PCBM. Using this approach, they reached a PCE of 20.8% as well as good stability. Li *et al.*[34] passivated the surface defects of perovskite film with reduced graphene oxide modified by 4-fluorophenylhydrazine hydrochloride (rGO-4FPH) and showed this to be due to the interaction between functional groups of rGO-4FPH and

coordinatively unsaturated Pb ions, resulting in a better photovoltaic property. Moreover, Zheng *et al.*[35] employed quaternary ammonium halides such as choline chloride to effectively mitigate surface ionic defects achieving a certified PCE of 20.59% with increased stability under humidity and light illumination.

Here we introduce adamantane (AD) and 1-adamantylamine (ADA) to mitigate defect states in PSCs. Adamantane is a colorless, crystalline solid, which is insoluble in water, but readily soluble in nonpolar organic solvents. Its melting point of 271 °C is unusually high for a hydrocarbon.[36] Adamantane and its derivatives form high-density self-assembled monolayers (SAMs) which have been used in molecular electronics, e.g. as barrier layers in tunnel junctions and for redox switchable dyads.[37] We show that surface modification of perovskite films by AD and ADA prolongs their photoluminescence lifetime by attenuating surface states acting as sites for nonradiative charge carrier recombination. As a consequence, ADA increases the V_{oc} by 60 mV to 1.17 V enabling a PCE of 21.3 % measured as stabilized power output under maximum power point tracking. Importantly, the surface treatment by ADA enhances greatly the stability of the PSC due to the unique film forming and strongly hydrophobic properties of the adamantane.

Results and Discussion

Figure 1a shows the structures for the AD and ADA molecules. The perovskite film is deposited from a triple A-cation perovskite solution containing formamidinium iodide (FAI), methyammonium iodide (MAI), and cesium iodide (CsI) by using anti-solvent method as specified in the method section. As shown in literature[38], triple A-cation perovskite suffers from small grain size and surface passivation is a good strategy to tackle this problem. The AD and

ADA additives were dissolved either in the anti-solvent (AS method) or spin coated on top of the perovskite (SC method) from chlorobenzene solution followed by drying at 120 °C for 10 min. Figure 1b and S1 show top-view SEM images of perovskite films before and after modification with AD and ADA modulators using AS and SC methods. From the images, it is clear that after AD and ADA treatment using both techniques, the average grain sizes are almost identical. The x-ray diffraction (XRD) patterns of perovskite films before and after passivation are shown in Figure 2a. The XRD patterns of perovskite layers modified by AD and ADA molecules remain the same as reference sample, which is similar to SEM results. The results suggest that the additives do not significantly affect the morphology of the perovskite film. The UV-visible and PL spectra of perovskite samples before and after surface modification by AD and ADA with optimum concentration of 1.5 mg/mL in CB are shown in Figure 2b. There is no discernable shift in the UV and PL peaks after incorporation of the additives inside the perovskite film whose band gap is about = 1.61 eV. Figure 2c depicts time resolved photoluminescence (TRPL) traces of perovskite films deposited on glass substrate before and after surface passivation with AD or ADA molecules. The PL decays were fitted to the stretched exponential function $I(t) = I_0\exp(-(t/\tau)^{\beta})$, where τ is the PL lifetime time and β is a stretch parameter. Table S1 shows the summary of fitting parameters for the PL decay curves. The PL lifetimes follow the order ADA > AD > reference illustrating that ADA is most effective in mitigating perovskite surface states acting as charge carrier recombination centers. To further study the role of passivation, Hall mobilities of perovskite films passivated by AD and ADA using AS and SC techniques were measured. As shown in Table S2, by applying these modulators, the mobilities for both techniques are increased. Our results confirm that this improvement for SC method is higher than AS one and ADA modulator is more effective than AD one.

Figure 3a shows the cross-sectional SEM image of the ADA treated PSCs on mesoporous TiO_2. The device structure consists of FTO glass covered by a 40 nm-thick compact TiO_2 blocking layer, a TiO_2 mesoporous scaffold with thickness of 150-200 nm, a 300 nm-thick perovskite film with, a layer of spiro-OMe-TAD as hole transport layer (200 nm), and an 80 nm-thick gold electrode as a back contact. Figure 3b shows the current density-voltage (*J-V*) curves of PSCs (forward and backward scan directions) before and after passivation with AD and ADA (with optimum concentration of 1.5 mg/mL in CB) by SC technique under simulated (AM1.5G) solar irradiation. The device parameters of champion cells are summarized in Table 1. The reference cell based on triple cation perovskite film gave a J_{sc} of 22.47 mA/cm^2, V_{oc} of 1.083 V, fill factor (*FF*) of 79.1%, and PCE of 19.32%. In contrast, AD-based device and ADA containing device exhibit significant improvement in V_{oc}. Thus, the PSC based on ADA treatment presents higher PCE up to 20.93% with J_{sc} of 22.57 mA/cm^2, V_{oc} of 1.155 V, and FF of 80.4%, while the AD-based solar cell shows the best performance of 20.47% (J_{sc} of 22.53 mA/cm^2, V_{oc} of 1.142 V, and FF of 79.3%). Notably, all PV parameters are improved by using AD and ADA molecules as additives. Nevertheless, from Figure 3b and Table 1, the V_{oc} emerges as the metric that profits the most from the ADA surface treatment with an impressive gain of 60 mV over the blank. Figure 3c shows the spectral response of the external quantum efficiency (EQE) of devices before and after passivation along with the projected photocurrent densities derived from calculating the overlap integral between the EQE spectrum and the standard AM 1.5 solar emission. The EQE values obtained with the AD and ADA treated samples are slightly higher than those of the reference cell in line with the measured photocurrents. The projected J_{sc} values agree well with the measured ones showing that any spectral mismatch between our simulator and the standard AM 1.5 emission is negligibly small.

Figure 3d shows the temporal evolution of the maximum power output of the reference cell and for the two PSCs based on surface treatment of the perovskite film with AD and ADA, respectively. The reference and the AD treated films show practically stable power output over the 60 second tracking time corresponding to 19.12 and 20.35 mW/cm^2, respectively. Conversely, the ADA modulated PSC shows an additional small rise in the output power until reaching a plateau corresponding to a stabilized PCE of 21.3 %. We infer from these measurements that the ADA surface treatment boosts the power conversion efficiency of our triple cation PSC by a remarkable 11.4 %.

In order to ascertain the reproducibility of the effects resulting from surface modification of the perovskite by the adamantanes we produced 30 devices, *i.e.* 10 for each category and checked the statistical variation of their PV parameters. Figure S2 shows the PV metrics obtained from the *J-V* curves of these cells. The results confirm the beneficial effect exerted by the surface treatment by AD and ADA on all the PV parameters the most striking being the enhancement of the V_{oc}. In addition, the results suggest that ADA is more effective in passivating the surface states of perovskite films than AD. We attribute this to stronger surface attachment of the ADA by virtue of its amine group that can anchor to the perovskite surface by replacing an A-cation or by filling an A cation vacancy. The presence of latter defects is undesirable as they act as hole traps immobilizing positively charged carriers at the interface between the perovskite and the spiro-OMeTAD. This enhances carrier recombination and causes hysteresis effects in the *J-V* curves because the trapped carriers produce a net local electric field that causes ion migration in the perovskite films. To further study the role of passivation, the electroluminescence (EL) of devices without and with passivation were measured. In this measurement, the voltage is changed from 0 to 1.3 V and reverse to plot a curve versus time. Figure S7 shows that the EL

signal for passivated devices with AD and ADA are stronger than the reference sample, confirming a lower level of defects promoting radiationless recombination in the absorber layer and interface, especially for ADA case.

The hysteresis indexes (h) of the passivated devices and reference cell were calculated from the formula $h = 100 \times (PCE_{backward} - PCE_{forward})/PCE_{backward}$. As shown in Figure S3, the hysteresis indexes of passivated devices are slightly lower than that of the reference cell.

Figure S4 demonstrates the histograms of the photovoltaic metrics of PSCs passivated with AD and ADA by using the antisolvent (AS) technique. From these measurements the AS treatment produces smaller performance benefits than spin coating the agents onto the perovskite surface.

In order to identify the optimal concentration of AD and ADA in the spin coating solvent we varied their content from 0 to 3 mg in 1 mL chlorobenzene and present the photovoltaic parameters of devices treated by these solutions in Figure S5 and S6. The data show that the best results are achieved for both additives with a concentration of 1.5 mg/mL in CB.

Table 1. Figure of merits for champion reference cell and passivated devices with AD and ADA modulators with optimum concentration of 1.5 mg/mL in CB under forward and backward scan directions

Sample	V_{oc} (V)	J_{sc} (mA/cm^2)	*FF* (%)	PCE (%)	Hysteresis index (%)
Reference-forward	1.081	22.43	78.1	19.01	1.65
Reference-backward	1.083	22.47	79.2	19.32	
Passivation with AD-forward	1.139	22.48	78.4	20.11	1.73
Passivation with AD-backward	1.142	22.53	79.3	20.47	
Passivation with ADA -forward	1.154	22.61	79.1	20.63	1.43

Passivation with ADA -backward	1.155	22.57	80.4	20.93	

* Note that the intensity of light was 0.998 sun in this measurement.

We further explored the role of adamantane additives and their location in perovskite film in the following manner. After passivation of perovskite film with AD and ADA, we spin-coated pure chlorobenzene five times on top of the passivated perovskite films and fabricated the PSC devices in the same condition as reference sample. The statistical photovoltaic data for the corresponding devices are shown in Figure S8. Interestingly our results show that by washing the surface of films, the V_{oc} is decreased slightly as compared to the samples without washing, indicating that these additives are present at the surface of the perovskite. Moreover, this V_{oc} loss for AD passivated film is larger than that of for ADA one. This result shows that ADA molecule has stronger bonding with the surface of perovskite film due to the presence of the amine group which can anchor to a A-cation vacancy. However, the photovoltaic results for washed samples are still better than the reference device (Figure S4). This indicates that the adamantane modulators are still available after washing the films and they do not penetrate far into the bulk of the perovskite bulk.

We measured the contact angle of water on top of the reference sample and the films passivated by AD and ADA and obtained the values of 35°, 56°, and 68°, respectively, as shown in Figure 4a-c. This implies that the films after passivation with AD or ADA have lower wettability by water molecules, protecting the perovskite film from water ingression which should enhance their stability.

We confirmed that the passivation of perovskite films with AD and ADA molecules does improve the PSC stability. We first examined the sensitivity of PSCs to humid air by placing

unsealed devices for 3 months in an air box with 20 % relative humidity. The result of this stability test is shown in Figure 4d. The perovskite whose surface was passivated with AD and ADA maintained 95% and 98% of their initial values, respectively, while the reference cell showed a 16% PCE loss. We subsequently exposed perovskite films on glass with and without surface passivation by the adamantanes to ambient atmosphere for 1 week. Figure 5a-c illustrates the photographs. The color of reference sample turned from black to yellow, indicating decomposition of perovskite film under formation of PbI_2. By contrast, the perovskite film passivated with ADA maintained its black colour while the one modified with AD discolored slightly. In order to further confirm the film quality, XRD patterns of the perovskite films before and after passivation were characterized. As shown in Figure 5d, the intensity of the PbI_2 peak located at 12.8° clearly depicts the decomposition of perovskite film under high humidity environment, which is the highest for reference sample.

We examined the operational stability of the PSCs by exposing them to continuous full-sun illumination under maximum power point tracking in a nitrogen atmosphere at T=30 °C. Figure 4e illustrates that devices treated with ADA and AD by the SC method retained 96% and 92% of their initial values after 300 h under continuous light illumination, respectively, while the reference sample incurred a 28% performance loss. Our investigations clearly show that the introduction of adamantanes as interfacial layers between the pervoskite film and the hole conductor is beneficial for both the performance and operational stability of state of the art perovskite solar cells.

Experimental Section

Device fabrication

FTO glass (NSG-10) was first etched by a chemical method using zinc powder and HCl solution (2 M). The substrates were cleaned by 20 min sonication in four steps using Triton X100 (1 vol% in deionized water), deionized water, acetone, and ethanol as cleaning liquids. Before deposition, all substrates were cleaned by UV/ozone for 15 min. To deposit the compact TiO_2 layer (c-TiO_2), titanium diisopropoxide acetyl acetonate (Sigma-Aldrich) was diluted in ethanol and deposited on substrates at 450 °C by using spray pyrolysis method, followed by 30 min annealing at 450°C. Thereafter, a 150 nm-thick mesoporous TiO_2 layer was spin coated on the c-TiO_2 (4000 rpm for 15 s with a ramp rate of 2000 rpm/s) using diluted TiO_2 paste (Dyesol 30 NR-D) in ethanol. Then, the substrates were annealed at 450°C for 30 min. After cooling the substrates to 150 °C, they were transferred to the glovebox for perovskite deposition. The precursor solution was prepared by mixing FAI (1.105 M, Dyesol), PbI_2 (1.16 M, TCI), MABr (0.195 M, Dyesol) and $PbBr_2$ (0.195 M, TCI), and CsI (0.068 M, TCI) in DMF:DMSO = 4:1 (volume ratio). The perovskite solution was spin-coated in two-step first at 1000 rpm for 10 s and, then at 4000 rpm for 30 s. During the second step, 200 μL of chlorobenzene (CB) anti-solvent was dropped on top of film 5 s before the end of spinning. Then, the film was annealed at 100 °C for 80 min. For passivation of perovskite film, the AD or ADA was either added to the anti-solvent chlorobenzene (AS method) or deposited by spin coating as separated layer (SC method). Thus, in the AS method, perovskite films were passivated during applying anti-solvent on top of the film before annealing, while in the SC technique, after annealing the perovskite film, various solutions of AD and ADA additives with different concentrations were deposited on top of perovskite layer by spin-coating at 4000 rpm for 30 s with a ramp rate of 2000 rpm/s. Afterward, the passivated films were annealed at 120 °C for 10 min. After annealing, spiro-OMeTAD solution in chlorobenzene (70 mM) containing bis(trifluoromethylsulfonyl)imide lithium salt (Li-TFSI, Sigma-Aldrich) solution (520 mg/mlacetonitrile) and (4-tert-butylpyridine-Sigma-Aldrich)

with molar ratios of 0.5 and 3.3, respectively, was prepared and spin-coated at 4000 rpm for 20 s with 2000 rpm/s ramp rate. Finally, the device structure was completed by thermal evaporation of 80-nm thick gold as an electrode with an active area of 0.16 cm^2.

Film characterization

The morphology of perovskite film, and device structure was studied using a ZEISS Merlin high resolution scanning electron microscopy (HRSEM). Quality and crystal structure of perovskite films were characterized by using X-ray diffraction (Bruker D8 X-ray Diffractometer, USA) utilizing a Cu $K\alpha$ radiation. For optical absorption measurement, a Varian Carry 500 spectrometer (Varian, USA) was used. To record steady-state photoluminescence spectra, an Edinburgh Instruments FLS920P fluorescence spectrometer, and for photoluminescence lifetime measurement (TRPL), a picosecond pulsed diode laser (EPL-405, excitation wavelength 405 nm, pulse width 49 ps) were employed. In order to analysis of TRPL results, PL decay curves were fitted to the following exponential function $I(t) = I_0 \exp(-(t/\tau)^{\beta})$, where τ is the decay time and β is a stretch parameter.

Device characterization

The solar cells were measured under AM1.5G sun simulator (a 450 W Xenon lamp (Oriel), with intensity of 100 $mWcm^{-2}$, equipped with a Schott K113 Tempax sunlight filter (Praezisions Glas & Optik GmbH) to simulate the emission spectra of AM1.5G standard in the region of 350-750 nm. Calibration of the lamp was performed using standard Silicon solar cell. To measure the current density-voltage (*J-V*) curves, a 2400 series source meter (Keithley, USA) instrument was employed. The voltage range for *J-V* sweeps was between 0 and 1.2 V, with a step size of 0.005 V and a delay time of 200 ms at each point. External quantum efficiency (EQE) spectra were measured with a commercial apparatus (Arkeo-Ariadne, Cicci Research s.r.l.) based on a 300

Watts Xenon lamp. Ecopia HMS 3000 setup (Microworld) with a magnetic field of 0.54 T in a 4-point configuration was used for Hall effect measurement. In addition, the thickness of the perovskite films was controlled by a profiler (Tencor Alpha step 500). A biologic MPG2 potentiostat and a white LED lamp were used to simulate full AM 1.5 Sun-equivalent for stability test. The stability measurement was performed in nitrogen atmosphere under continuous light illumination using a device with active area of masked to 0.16 cm^2. The maximum power point (MPP) and *J-V* curve of devices were recorded every 10 s and every 10 min, respectively.

Supporting Information

Supporting information is available from the Wiley online library or from the author.

Acknowledgements

M.M.T would like to thank school of engineering of Hong Kong University of Science and Technology for their support. MG and SMZ thank funding from the European Union's Horizon 2020 program, through a FET Open research and innovation action under grant agreement No 687008.

Conflict of Interest

The authors declare no conflict of interest.

Keywords

Passivation, Adamantane, Perovskite, Solar cell, Stability

References

[1] J. W. Lee, H. S. Kim, N. G. Park, *Acc. Chem. Res.* **2016**, *49*, 311.

[2] W. S. Yang, B. W. Park, E. H. Jung, N. J. Jeon, Y. C. Kim, D. U. Lee, S. S. Shin, J. Seo, E. K. Kim, J. H. Noh, S. I. Seok, *Science* **2017**, *356*, 1376.

[3] https://www.nrel.gov/pv/assets/images/efficiency-chart.png

[4] A. Ng, Z.Ren, Q.Shen, S. H. Cheung, H. C.Gokkaya, S. K. So, A. B. Djurišić, Y. Wan, X. Wu, C. Surya, *ACS Appl. Mater. Interfaces* **2016**, *8,* 32805.

[5] J. Burschka, N. Pellet, S. J. Moon, R. Humphry-Baker, P. Gao, M. K. Nazeeruddin, M. Grätzel, *Nature* **2013**, *499*, 316.

[6] M. M. Tavakoli, R. Tavakoli, S. Hasanzadeh, M. H. Mirfasih, *J. Phys. Chem. C* **2016**, *120*, 19531.

[7] T. Li, Y. Pan, Z. Wang, Y. Xia, Y. Chen, W. Huang, *J. Mater. Chem. A* **2017**, *5*, 12602.

[8] X. Li, D. Bi, C. Yi, J. D. Décoppet, J. Luo, S. M. Zakeeruddin, A. Hagfeldt, M. Grätzel, *Science* **2016**, *353*, 58.

[9] X. Li, M. I. Dar, C. Yi, J. Luo, M. Tschumi, S. M. Zakeeruddin, M. K. Nazeeruddin, H. Han, M. Grätzel, *Nat. Chem.* **2015**, *7,* 703-711.

[10] M. Saliba, T. Matsui, K. Domanski, J. Y. Seo, A. Ummadisingu, S. M. Zakeeruddin, J. P. Correa-Baena, W. R. Tress, A. Abate, A. Hagfeldt, M. Grätzel, *Science* **2016**, *354,* 206.

[11] W. Nie, H. Tsai, R. Asadpour, J.-C. Blancon, A.-J. Neukirch, G. Gupta, J.-J. Crochet, M. Chhowalla, S. Tretiak, M.-A. Alam, H. -L. Wang, A.-D. Mohite, *Science* **2015**, *347*, 522.

[12] P. Liang, C. Liao, C. Chueh, F. Zuo, S. -T. Williams, X. Xin, J. Lin, A.-K.-Y. Jen, *Adv. Mater.* **2014**, *26,* 3748.

[13] M.-M. Lee, J. Teuscher, T. Miyasaka, T. -N. Murakami, H.-J. Snaith, *Science* **2012**, *338*, 643.

[14] Y. Zhao, J. Wei, H. Li, Y. Yan, W. Zhou, D. Yu, Q. Zhao, *Nat. Commun.* **2016**, *7*, 10228.

[15] J. Wei, H. Li, Y. Zhao, W. Zhou, R. Fu, Y. Leprince-Wang, D. Yu, Q. Zhao, *Nano Energy* **2016**, *26*, 139.

[16] Y. Shao, Z. Xiao, C. Bi, Y. Yuan, J. Huang, *Nat. Commun.* **2014**, *5*, 5784.

[17] J. Xu, A. Buin, A.-H. Ip, W. Li, O. Voznyy, R. Comin, M. Yuan, S. Jeon, Z. Ning, J.-J. McDowell, P. Kanjanaboos, J. Sun,X. Lan, L.-N. Quan, D.-H. Kim, I.-G. Hill, P. Maksymovych, E.-H. Sargent, *Nat. Commun.* **2015**, *6*, 7081.

[18] E. Edri, S. Kirmayer, A. Henning, S. Mukhopadhyay, K. Gartsman, Y. Rosenwaks, G. Hodes, D. Cahen, *Nano Lett.* **2014**, *14*, 1000.

[19] S. Delbos, *EPJ Photovoltaics* **2012**, *3*, 35004.

[20] K.-M. Boopathi, R. Mohan, T. Huang, W. Budiawan, M. Lin, C. Lee, K. Ho, C. Chu, *J. Mater. Chem. A* **2016**, *4*, 1591.

[21] S. Bag, M.-F. Durstock, *ACS Appl. Mater. Interfaces* **2016**, *8*, 5053.

[22] J.-H. Heo, D.-H. Song, H.-J. Han, S.-Y. Kim, J.-H. Kim, D. Kim, H.-W. Shin, T.-K. Ahn, C. Wolf, T. Lee and S.-H. Im, *Adv. Mater.* **2015**, *27*, 3424.

[23] J. Kim, J.-S. Yun, X. Wen, A.-M. Soufiani, C.-F.-J. Lau, B. Wilkinson, J. Seidel, M. -A. Green, S. Huang, A.-W.-Y. Ho-Baillie, *J. Phys. Chem. C* **2016**, *120*, 11262.

[24] C. Liu, X. Hu, C. Zhong, M. Huang, K. Wang, Z. Zhang, X. Gong, Y. Cao, A. J. Heeger, *Nanoscale* **2014**, *6*, 14297.

[25] M. Su, C. Kuo, M. Yuan, U. Jeng, C. Su, K. Wei, *Adv. Mater.* **2011**, *23*, 3315.

[26] P. Docampo, F.-C. Hanusch, S.-D. Stranks, M. D¨oblinger, J.-M. Feckl, M. Ehrensperger, N.-K. Minar, M.-B. Johnston, H. -J. Snaith, T. Bein, *Adv. Energy Mater.* **2014**, *4*, 1400355.

[27] Y. Zhao, K. Zhu, *J. Am. Chem. Soc.* **2014**, *136*, 12241.

[28] Y. Xie, F. Shao, Y. Wang, T. Xu, D. Wang, F. Huang, *ACS Appl. Mater. Interfaces* **2015**, *7*, 12937.

[29] M. Yang, T. Zhang, P. Schulz, Z. Li, G. Li, D.-H. Kim, N. Guo, J.-J. Berry, K. Zhu, Y. Zhao, *Nat. Commun.* **2016**, *7*, 12305.

[30] S. Li, C. Chang, Y. Wang, C. Lin, D. Wang, J. Lin, C. Chen, H. Sheu, H. Chia, W. Wu, U. Jeng, C. Liang, R. Sankar, F. Chou, C. Chen, *Energy Environ. Sci.* **2016**, *9*, 1282.

[31] Y. Matsuo, Y. Sato, T. Niinomi, I. Soga, H. Tanaka, E. Nakamura, *J. Am. Chem. Soc.* **2009**, *131*, 16048.

[32] D. Bi, C. Yi, J. Luo, J. D. Décoppet, F. Zhang, S. M. Zakeeruddin, X. Li, A. Hagfeldt, M. Grätzel, *Nat. Energy* **2016**, *1*, 16142.

[33] F. Zhang, W. Shi, J.Luo, N. Pellet, C. Yi, X. Li, X. Zhao, T. J. S. Dennis, X. Li, S. Wang, Y. Xiao, S. M. Zakeeruddin, D. Bi, M. Gratzel, *Adv. Mater.* **2017**, *29,* 1606806.

[34] H. Li, L. Tao, F. Huang, Q. Sun, X. Zhao, J. Han, Y. Shen, M. Wang, *ACS Appl. Mater. Interfaces* **2017**, *9*, 38967.

[35] X. Zheng, B. Chen, J. Dai, Y. Fang, Y. Bai, Y. Lin, H. Wei, X. C. Zeng, J. Huang, *Nat. Energy* **2017**, *2*, 102.

[36] C. E. Nordman, D. L. Schmitkons, *Acta Crystallographica* **1965**, *18*, 764.

[37] T. Kitagawa, H. Matsubara, K. Komatsu, K. Hirai, T. Okazaki, T. Hase, *Langmuir* **2013**, *29,* 4275.

[38] M. Saliba, T. Matsui, J. Y. Seo, K. Domanski, J. P. Correa-Baena, M. K. Nazeeruddin, S. M. Zakeeruddin, W. Tress, A. Abate, A. Hagfeldt, M. Grätzel, *Energy Environ. Sci.* **2016**, *9,* 1989.

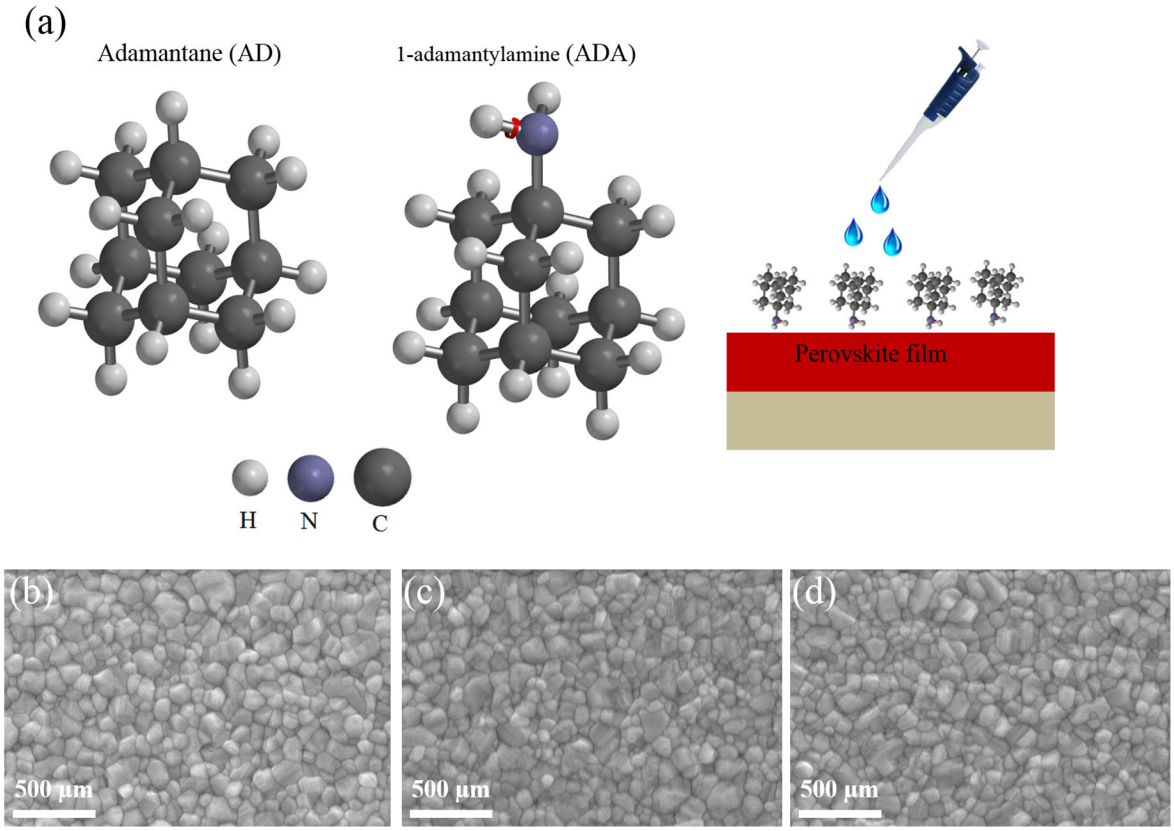

Figure 1. (a) Chemical structure of adamantane (AD) and 1-adamantylamine (ADA) used for passivation of perovskite film. Top-view SEM images of perovskite films modified by SC technique based on (b) pure CB, (c) AD, and (d) ADA (The concentrations of both AD and ADA modulators were 1.5 mg/mL).

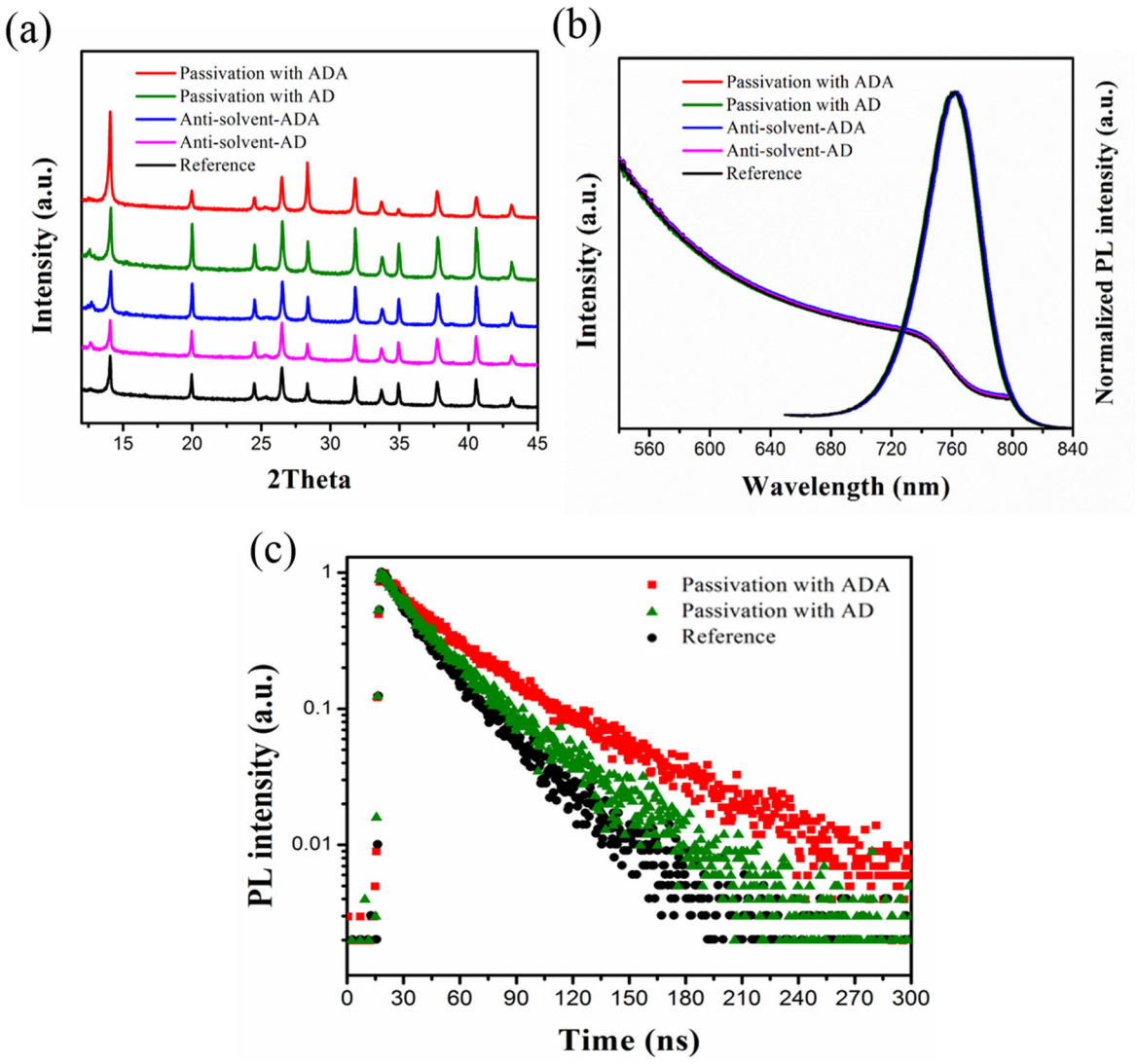

Figure 2. (a) XRD patterns of perovskite films passivated with AS and SC techniques. (b) UV-visible and PL spectra, and (c) TRPL spectra of perovskite films before and after passivation by AD and ADA molecules with optimum concentration of 1.5 mg/mL in CB using SC method.

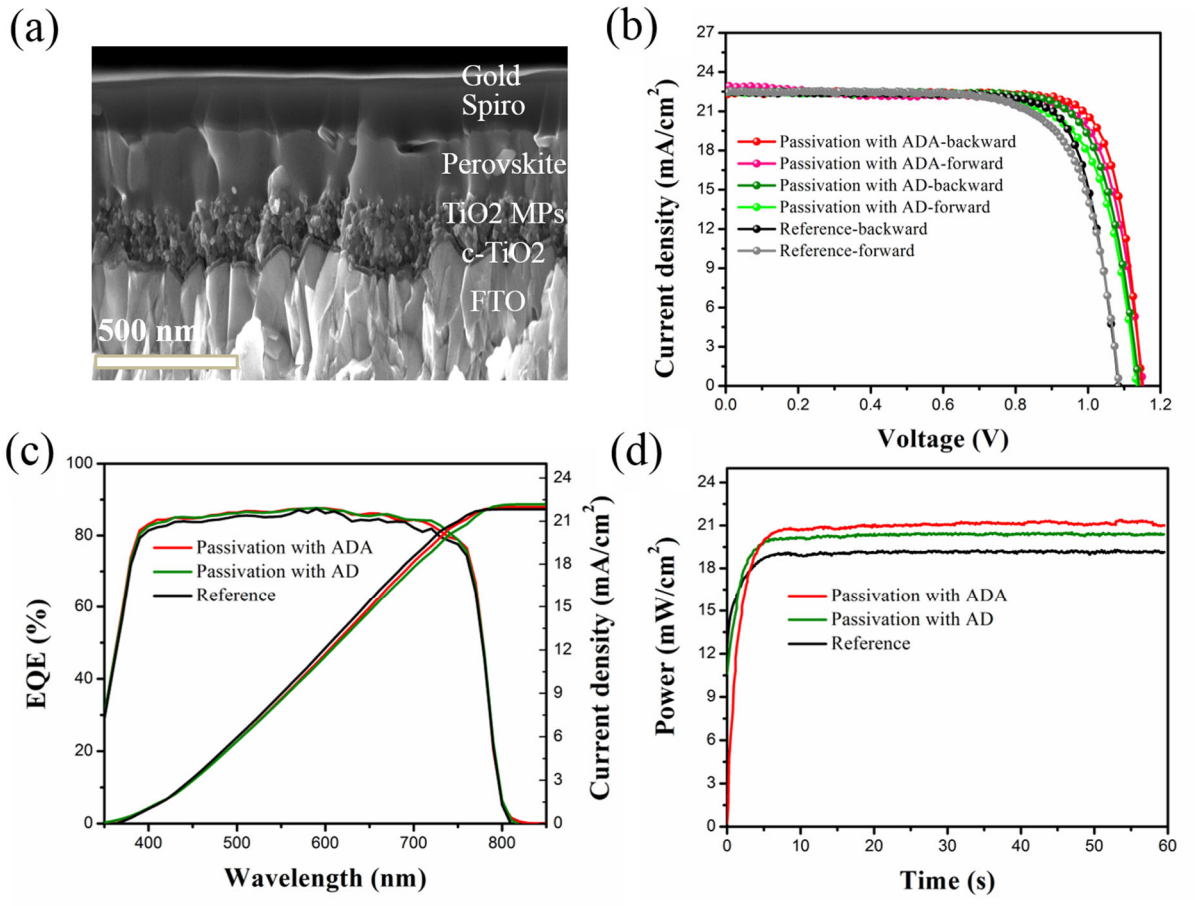

Figure 3. (a) Cross-sectional SEM image of PSC based on mesoporous TiO_2 scaffold and ADA passivation. (b) Solar cells comprising champion devices before and after passivation by AD and ADA with optimum concentration of 1.5 mg/mL in CB using SC technique under both backward and forward scan direction. (c) External quantum efficiency (EQE) spectra and integrated current density curves of the corresponding devices. (d) Stabilized power output of the corresponding devices.

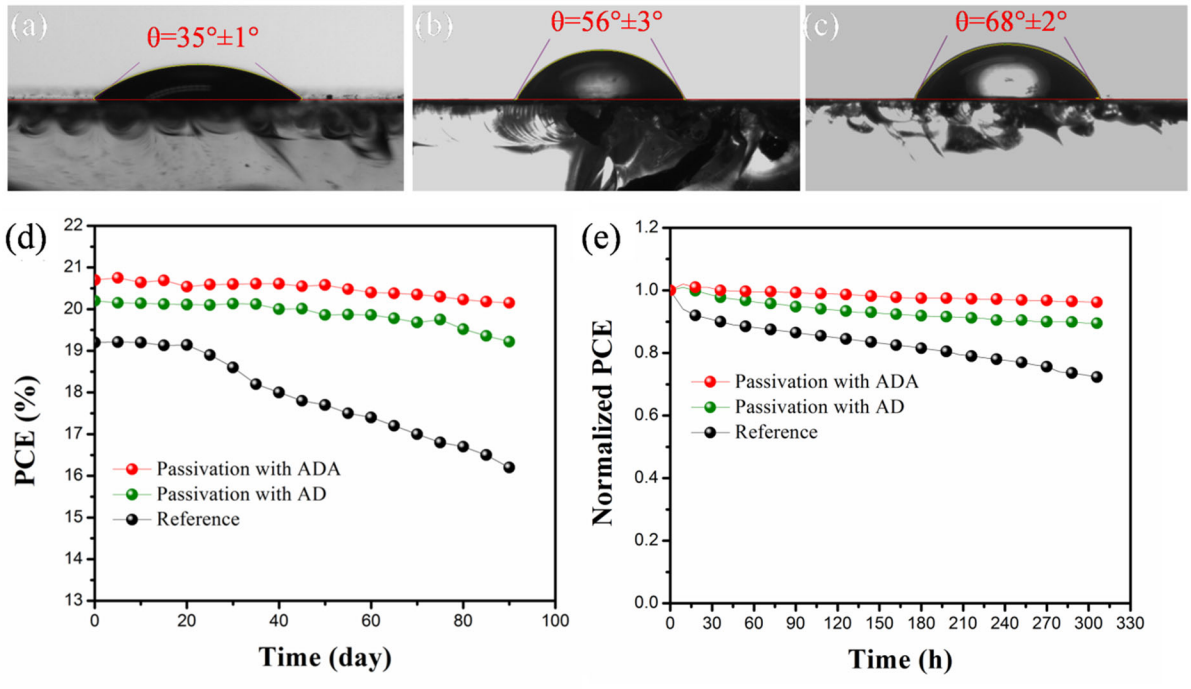

Figure 4 Contact angle measurement of water droplet on top of perovskite films: (a) reference sample, (b) AD-passivated film, (c) ADA-passivated film. (d) Stability test of corresponding PSCs in an ambient environment with 20% relative humidity. (e) Stability test of PSCs with and without passivation under continuous full-sun illumination and maximum power point tracking in a nitrogen atmosphere at T=30 °C (the concentration of AD and ADA modulators were 1.5 mg/mL in CB).

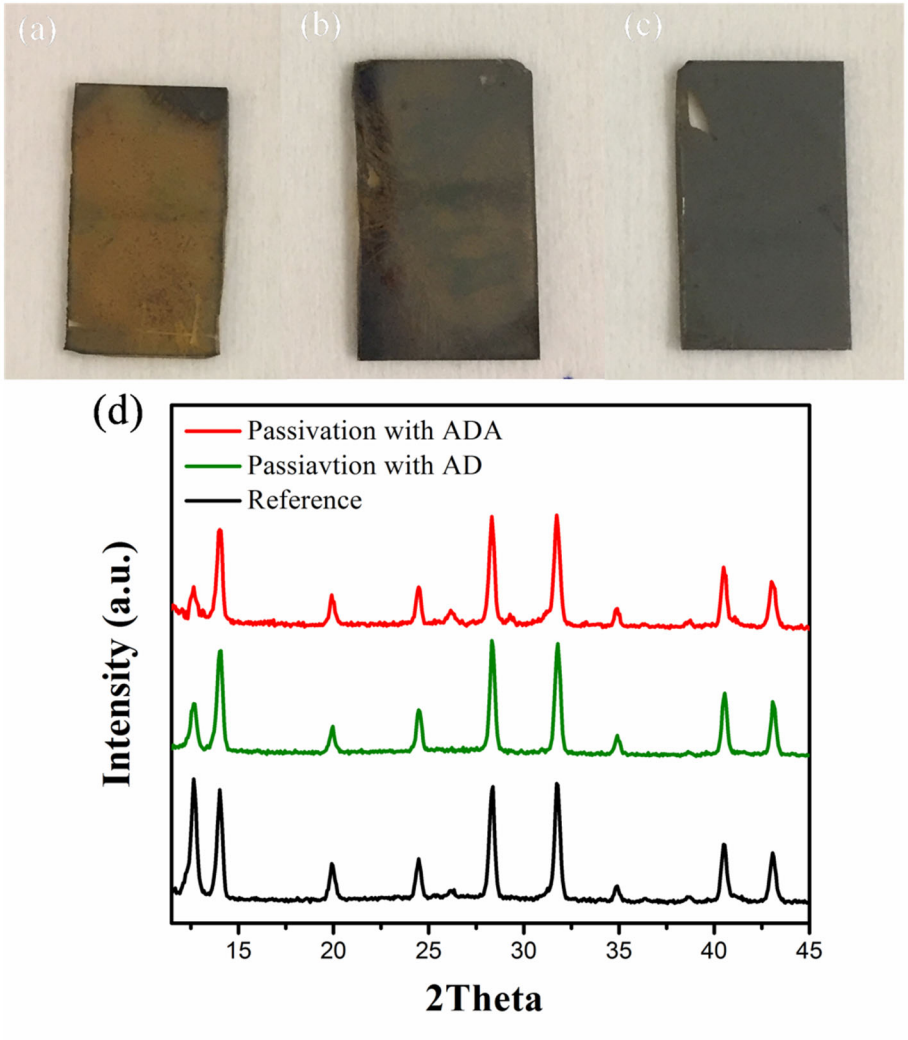

Figure 5. Humidity test for perovskite films before and after passivation by AD and ADA with optimum concentration of 1.5 mg/mL in CB: Maintaining of the perovskite films at relative humidity of 65% for one week, (a) reference sample, (b) AD-passivated, and (c) ADA-passivated perovskite films. (d) XRD patterns of the corresponding perovskite films after keeping them at 65% humidity for one week.

TOC graphic

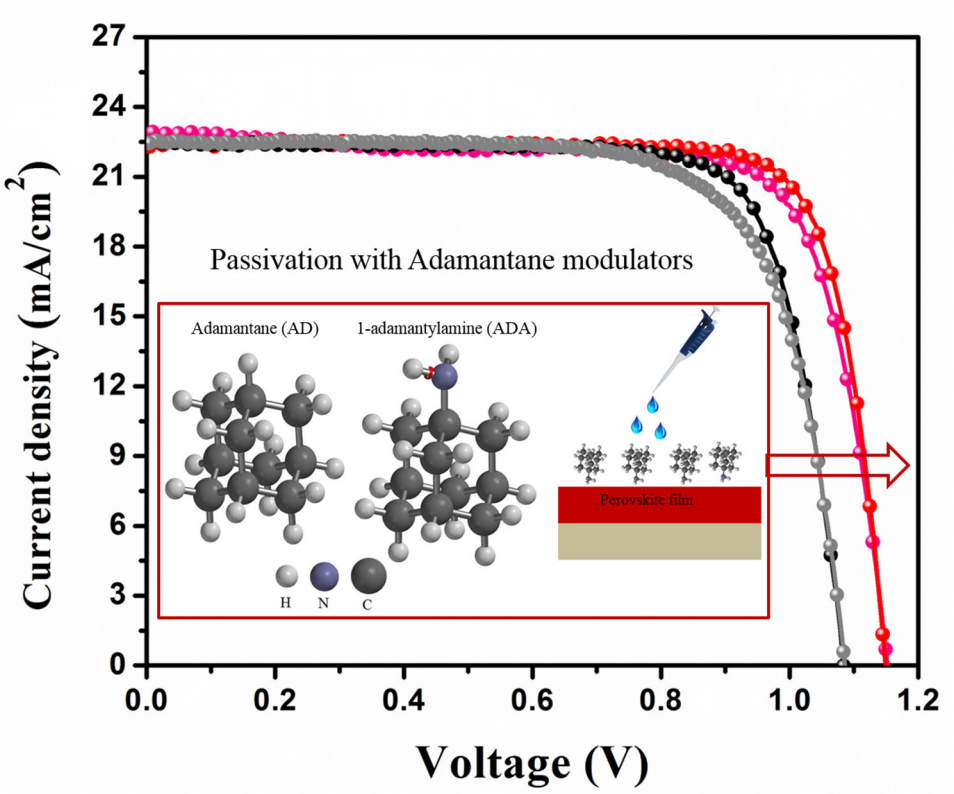

The introduction of Adamantane modulators as an interfacial layer between perovskite and hole transporting layer enhance the photovoltaic performance and operational stability of state of the art perovskite solar cells by effective mitigation of interfacial defect states.